RC23090 (W0401-140) January 29, 2004
Electrical Engineering

IBM Research Report

Extraction of $\varepsilon_r(f)$ and tan $\delta(f)$ for Printed Circuit Board Insulators up to 30 GHz Using the Short-Pulse Propagation Technique

A. Deutsch, T.-M. Winkel[1], G. V. Kopcsay, C. W. Surovic, B. J. Rubin, G. A. Katopis[2], B. J. Chamberlin[3], R. S. Krabbenhoft[4]

IBM Research Division
Thomas J. Watson Research Center
P.O. Box 218
Yorktown Heights, NY 10598

[1]IBM Laboratory
7032 Boeblingen
Germany

[2]IBM Server Group
Poughkeepsie, NY 12601

[3]IBM Microelectronics Division
Endicott, NY 13760

[4]IBM Server Group
Rochester, MN 55901

Research Division
Almaden - Austin - Beijing - Haifa - India - T. J. Watson - Tokyo - Zurich

Extraction of $\varepsilon_r(f)$ and tan $\delta(f)$ for Printed Circuit Board Insulators up to 30 GHz Using the Short-Pulse Propagation Technique

A. Deutsch, T-M. Winkel[1], G. V. Kopcsay, C. W. Surovic, B. J. Rubin, G. A. Katopis[2], B. J. Chamberlin[3], R. S. Krabbenhoft[4]

IBM T. J. Watson Research Center, P. O. Box 218, Yorktown Heights, N.Y. 10598,
Phone: (914) 945-2858, Fax: (914) 945-2141, email:deutsch@us.ibm.com
[1]IBM Laboratory, 7032 Boeblingen, Germany
[2]IBM Server Group, Poughkeepsie, NY 12601
[3]IBM Microelectronics Division, Endicott, NY 13760
[4]IBM Server Group, Rochester, MN 55901

Abstract **–** In this paper, the self-consistent, frequency-dependent dielectric constant, $\varepsilon_r(f)$, and dielectric loss, tan$\delta(f)$, of several materials are determined over the range 2 to 30 GHz using a short-pulse propagation technique and an iterative extraction based on a rational function expansion. The simple measurement technique is performed in the time domain on representative printed-circuit board wiring. Broadband, fully-causal transmission-line models based on these results are generated up to 50 GHz for card wiring using low loss materials including BT, Nelco N4000-13, and Nelco N4000-13SI. Simulation and modeling results highlight the need for the accurate frequency-dependent dielectric loss extraction. Signal propagation based on these results shows very good agreement with measured step and pulse time-domain excitations and provides validation of the measurement and model generation technique.

Keywords **–** Dielectric loss extraction, lossy causal transmission line models, short-pulse propagation measurement technique, printed circuit board characterization.

Introduction

Continued advances in the clock frequencies and data-rates of high-performance digital systems require increasingly more accurate interconnection modeling capability [1,2]. Enhanced models for transmission-lines that propagate multi-GHz signals depend upon accurate material parameter characterization. Therefore, measurement bandwidth needs to extend into the many tens of GHz. Slower risetimes used in the past were tolerant of less accuracy or even non-causal models; for multi-GHz operation, the broad spectral content is generating renewed interest in enhanced measurement techniques. Moreover, new materials for printed circuit board wiring are being developed in order to make possible high-bandwidth signal transmission. These new materials need to be accurately characterized in configurations that are representative of actual use. This poses new challenges to the standard frequency-domain techniques used in the past [3]; several attempts have been made to use a combination of techniques over different frequency ranges to cover the entire spectrum of interest [4,5]. A promising transmission-line based technique has been shown on lines with much smaller discontinuities as found on chip [6].

A very promising class of materials is based on the blending of bismaleimide triazine (BT) and epoxy-resin to provide enhanced thermal, mechanical and electrical performance for use in printed circuit board wiring. In this paper, the short-pulse propagation technique first introduced in [7] is extended to extract the complex permittivity for BT-based card wiring up to 30 GHz, and simulations using causal transmission-line models with these material characteristics are compared with time-domain measurements on representative structures. Specially designed test vehicle structures are shown that enabled this increase in measurement bandwidth and the frequency-dependent extraction. The fitting technique used for the broadband extraction of $\varepsilon(f)$ and tan$\delta(f$ is also briefly described. Additional results are shown for two other newer low-loss, multifunctional epoxy materials, namely Nelco N4000-13 [8] and Nelco N4000-13SI [8]. The need for broadband accurate dielectric loss extraction is highlighted with simulations of various wiring cross sections.

Measurement Technique

The bandwidth of the short-pulse propagation technique has been shown to be extendable up to 70 GHz [9] given a very fast excitation-source and low-loss transmission-lines. For realistic printed-circuit board configurations, however, this measurement bandwidth has generally been limited to less than 10 GHz [10]. In this study, we show that careful design of the test structures allows 30 GHz measurement bandwidth even for fairly lossy card wiring. Moreover, a new fitting algorithm is combined with the data obtained from the short-pulse propagation and low frequency parallel-plate capacitance measurements to extract broadband complex permittivity. The technique is implemented on recently developed, lower-loss printed circuit board materials and fully-causal transmission line models are generated up to 50 GHz.

The measurement technique employs a short, electrical pulse that is launched onto a transmission-line structure. This pulse is obtained by differentiating the step-source of a sampling oscilloscope (HP model 54120A) using a passive impulse-forming network (Picosecond Pulse Labs model 5208). High-speed coaxial probes in ground-signal (GS) configuration, (GGB Industries model 40A, 150LP) are used to connect to the transmission-lines. The transmitted pulse is detected and digitized. The 50-GHz sampling oscilloscope detector channel is used with 2.4 mm connectors and 40 GHz flexible coaxial cables (Gore GD/AJ, 160-mil-diameter) between the probes and the oscilloscope. A source pulse of 35 ps width was launched on lines with 1.0 and 9.8 cm, and 2.0 and 8.0 cm lengths. In addition, a 29 ps width pulse (obtained with the Picosecond Pulse Labs pulse generator 4015C and the 5208 network) was launched on lines with 1 and 5 cm lengths. The stripline cross section described later is shown in Fig. 7. The measured propagated pulse widths were 37 and 49 ps, 39 and 45

ps, and 30 and 36 ps, respectively. Two such pulses are shown in Fig. 1. Time windowing is performed on the digitized pulses in order to eliminate any unwanted reflections from probes, pads, vias, and cable connectors. Since amplitude resolution is more essential than spectral resolution, rectangular windowing is used with a smooth transition to the signal baseline steady-state levels. These processed waveforms are Fourier transformed, and the ratio of the complex spectra yields the propagation constant

$$\Gamma(f) = \alpha(f) + j\beta(f) = \frac{1}{l_1 - l_2} \ln \frac{A_1(f)}{A_2(f)} + j \frac{\Phi_1(f) - \Phi_2(f)}{l_1 - l_2} \tag{1}$$

where $\alpha(f)$ and $\beta(f)$ are the frequency-dependent attenuation coefficient and phase constant, respectively. $A_i(f)$ and $\Phi_i(f)$ (i=1,2) are the amplitude and phase of the transforms corresponding to lines of lengths l_1 and l_2, respectively, with $l_1 > l_2$. No de-embedding or calibration is required since the effects of interface discontinuities simply cancel out or are eliminated by the windowing process. The characteristic impedance can be obtained from

$$Z_0(\omega) = \Gamma(\omega) / [\, G(\omega) + j\omega C(\omega)] \tag{2}$$

The implicit assumption is that measured transmission-lines of lengths l_1 and l_2 have very similar characteristics and are uniform over their entire length since this extraction obtains effective per-unit-length (p.u.l.) parameters.

In general, C and G are frequency dependent and are related by a Hilbert transform due to causality as explained in [1, 2]. A causal response implies that the complex permittivity, $\varepsilon(\omega) = \varepsilon'(\omega) - j\varepsilon''(\omega)$ has a real part that is an even function of frequency and an imaginary part that is an odd function. Therefore, $\varepsilon'(-\omega) = \varepsilon'(\omega)$ and $\varepsilon''(-\omega) = -\varepsilon''(\omega)$, and $\tan\delta = \varepsilon'' / \varepsilon'$ is also an odd function of frequency. It should be noted that many previous printed circuit board analyses have assumed that both ε_r and $\tan\delta$ are frequency independent. In order to obtain $C(\omega)$ and $G(\omega)$, accurate knowledge of material parameters over a wide frequency range is needed. Such data is very difficult to obtain, and generally several measurement techniques are used, each optimized for specific frequency bands [3, 4]. Many of these techniques might not be possible with actual stripline configurations.

In order to circumvent this problem, the following methodology was used. The stripline transmission-lines tested were cross-sectioned, and actual dimensions were used for modeling the structure. Four port measurements were used to obtain the dc resistance of the sample lines, R = 0.18 Ω/cm. Copper resistivity, ρ = 2.266 μΩ–cm, was calculated using the measured dimensions. At low frequency, the real part of the complex permittivity, $\varepsilon = \varepsilon^*_r \varepsilon_0 = \varepsilon_0 [\varepsilon'_r - j\varepsilon''_r]$, was obtained from capacitance and dissipation factor measurements, and from the insulator thickness. A 1.27 cm (500 mil) diameter, circular plate (shown in Fig. 7c), embedded in the signal layer of the stripline structure was measured with a Multi-Frequency LCR Meter (HP model 4275A). Because of the large diameter-to-height insulator ratio (> 100), fringe capacitance could be ignored. The value obtained was ε'_r = 3.75 at 1 MHz as shown in Table I. The p.u.l. $R(\omega)$ and $L(\omega)$ were also calculated using the known dimensions and copper resistivity from 10 kHz to 50 GHz. The effect of surface roughness was not taken into account. An initial set of values was assumed for the loss tangent of the dielectric, $\tan\delta = \varepsilon''_r / \varepsilon'_r$ along with the real ε'_r value measured at 1 MHz. An analytic function based on the Debye model for the complex permittivity [1, 4, 5] was used to interpolate between the specified $\tan\delta$ points as described below.

When interpolating dielectric constant data, it is necessary to insure consistency between the real and imaginary parts of the resulting approximation to produce a causal response. In principle, if either the real or imaginary part is known, the other can be obtained via a Hilbert transform. However, the data would need to be known at all frequencies. Alternatively, by using an interpolation function with analytic properties that insure the real and imaginary parts are causally related, the technique described here avoids the necessity of applying a Hilbert transform. This interpolating function consists of a finite series of rational terms with self-consistent real and imaginary parts as shown in equation (3), with coefficients chosen to fit the measured total loss behavior over the desired frequency range. This fit is not based on any specific physical resonances in the material. Equation (3) contains 2 n + 1 adjustable parameters since the relaxation times and the amplitudes may be specified independently. An inspection of the sum (3) shows that each term contributes to the imaginary part of the dielectric constant only near the pole frequency $1/\tau_i$. Since we know the range of frequencies that the approximate dielectric function is intended to cover, we can pre-specify these relaxation times appropriately. Amplitudes can then be found via a simple linear equation solution. We typically use a piecewise linear expansion of the given loss data versus $log(f)$ to provide estimates of the dissipation factor at the specified pole frequencies to generate a sufficient set of equations. The procedure can be iterated to adjust the fit.

$$\varepsilon(\omega) = \varepsilon_\infty + \sum_i \frac{\varepsilon_i}{1 + j\omega\tau_i} \tag{3}$$

Once an initial dielectric fit is obtained, the total measured and calculated attenuation are compared, and parameters of the expansion $(\varepsilon_\infty, \varepsilon_i, \tau_i)$ in (3) are adjusted to improve the fit. Only a few frequency points are usually needed to determine an

acceptable fit, since most useful card insulators have a slowly varying frequency dependence of both ε_r' and tan δ. The interpolated values can be extended smoothly over the desired frequency range. Since the low-frequency C measurement of the circular plate can typically be made with ±1% accuracy at 1 MHz where the errors caused by parasitics of leads, probes, pads, and vias are small, the constant parameter ε_∞ in the expansion was adjusted such that the fit matched the extracted ε_r' at 1 MHz [1]

Dielectric loss results in an increasing capacitance with decreasing frequency. This slow capacitance variation, that is necessary for causality, increases approximately in inverse proportion to *log(f)* over a wide frequency range. At low frequencies, G is very small (since it is proportional to frequency), and thus does not contribute significantly to the overall transmission line loss. At high frequency the value of G approaches a constant value in our approximation due to the finite number of poles used in the representation. The fit is extrapolated over the frequency range of 10 KHz to 50 GHz that is adequate for the spectral content of the representative digital signals. For use in typical circuit simulators, where all signals are bandlimited, it is sufficient to represent transmission lines over the frequency range that contains all significant signal energy. The interpolated complex dielectric constant determines $C(\omega)$ and $G(\omega)$ which are then used to calculate the attenuation constant $Att = 20\log_{10} e^{Re\Gamma(\omega)}$ where

$$\Gamma(\omega) = \sqrt{(R(\omega) + j\omega L(\omega))(G(\omega) + j\omega C(\omega))} \tag{4}$$

This attenuation is compared with the measured vales as shown in Fig. 2. Similarly, the phase constant, shown in Fig. 3, is obtained from $\beta(\omega) = Im\Gamma(\omega)$. This process is iterated a few times until good agreement is obtained. Typical starting values for tan δ are in the range of 0.005 – 0.025 since higher values would not be of interest for materials used in card wiring. Low-frequency dissipation factor values were also obtained for the circular plate in the range 10 KHz to 1 MHz and added to the few points used in the high range and shown in Table I.

Data obtained from the short-pulse measurement covered the frequency range of 1.95 GHz – 30 GHz. The fitted data was smoothly joined with the low frequency measurement data down to 10 KHz. The high frequency range was extrapolated from 30 to 50 GHz based on the assumption that material parameters are slowly varying with frequency. In order to cover the range of 1.95 – 30 GHz, three sets of short-pulse measurements were needed, namely with l_1 = 8 cm and l_2 = 2 cm, with l_1 = 9.8 cm and l_2 = 1 cm, and with l_1 = 5 cm and l_2 = 1 cm. The spectral content for the three sets were 2.3 GHz – 26 GHz, 1.95 GHz – 20 GHz, and 3.8 GHz to 30 GHz, respectively. Comparison of these three sets of data allowed us to compensate for inaccuracies caused by the imperfect cancellation of the effects of interface discontinuities when taking the ratio of the two Fourier transforms for the lines l_1 and l_2. These different sets of data include losses for different lengths of lines and the effect of these losses on the bandwidth of the measurement. Some of the ripples seen on the measured attenuation in Fig. 2 are caused by the lack of cancellation and the limitations of the windowing process.

The calculated line capacitance value using the measured ε_r' = 3.75 obtained at 1 MHz was C_{1MHz} = 1.449 pF/cm while the measured result was C_{1MHz} = 1.411 pF/cm. This good agreement gave one more validation measure. The calculated $C(\omega)$ and $G(\omega)$ that gave the acceptable agreement shown in Fig. 2 were used to extract the frequency-dependence shown in Fig. 4. Here $\varepsilon_r'(\omega) = C(\omega)/C_{1MHz}$ x 3.75 and tan $\delta(\omega) = G(\omega)/\omega C(\omega)$. This allowed the extraction of $\varepsilon_r'(\omega)$ and tan $\delta(\omega)$ over the frequency range 10 KHz to 30 GHz. Two other materials were also analyzed, namely Nelco N4000-13 and Nelco N4000-13SI. All three materials have much smaller loss than FR4 and the Nelco N4000-13SI exhibits the least variation with frequency for the dielectric loss as seen in Fig. 5. These smoothly extrapolated data were used (Fig. 4) to generate transmission-line parameters up to 50 GHz. To accurately simulate the high-speed digital signals of interest, extracted $\varepsilon_r'(\omega)$ and tan $\delta(\omega)$ are needed with good accuracy in the 1 – 50 GHz range. The low-frequency points are added in order to generate broadband consistent models, but their effect on the high-speed signal propagation is usually not significant since skin effect losses are dominant at typical signal frequencies. Thus, by using the above techniques a relatively small number of actual data points obtained via different measurement techniques can be combined to generate broadband transmission line models that are suitable for performance prediction of digital signaling.

Measurement Limitations

Due to the frequency dependence of dielectric attenuation, accuracy of the extracted tan δ is limited by the amplitude resolution of the measurement. Above about 4 GHz for typical materials we can resolve changes in dissipation factor of less than 5%.. The extraction resolution is approximately proportional with frequency for materials with slowly varying dielectric loss. For example, the resolution is only about 10% at 2 GHz as shown in Fig. 6. The high frequency limit of this measurement is determined by signal to noise ratio of the measurement set-up, given the spectral content of the pulse width that can be propagated through the line. In addition, as frequency increases additional uncertainty is introduced since, as mentioned above, no correction has been made for surface roughness in calculating the conductor loss. Nevertheless, the measured total attenuation and impedance of the line are matched accurately by the resulting transmission line models as shown below and ultimately this is what is used in simulations for signal performance predictions. The technique is also limited if the interface discontinuities are too large to be canceled either by windowing or by the ratioing operation. Large reflections also limit the extent of the window used and thus the low-frequency limit. Line non-uniformity can also introduce

inaccuracy. Since it is a time-domain technique, it is difficult to assess the accuracy at any particular frequency due to the broad spectral content of the measured pulses. Time-domain detectors available in typical sampling oscilloscopes have a noise floor that increases with frequency, and the spectral content of the measured signals decreases. On the other hand, the accuracy of frequency-domain s-parameter measurements is affected by calibration and de-embedding. Accuracy can be determined at any particular frequency, however, if the accuracy suffers for the higher-frequency points, when all the frequencies are used to reconstruct time-domain data, then the created pulses will have embedded error. The noise floor for each frequency, however, can be improved by filtering and thus generally is much lower. We have verified that the attenuation measurement had very good repeatability. For example, at 1.5 GHz, we found a +/-6% reproducibility from measurements made at different times, on the same sample, even with different probes.

Validation of Results

Wide-bandwidth extraction of $\varepsilon_r'(\omega)$ and $\tan\delta(\omega)$ was enabled by use of a special test vehicle. It consisted of a very thin, 635 μm (25 mil), printed-circuit card, containing one signal layer between two ground planes with 203.2 μm (8 mil) diameter vias that connect to the top-surface test pads as shown in Figs. 7a and b. Specially designed test pads are shown in Figs. 8a and b, and the two ground planes are connected with vias on 1016 μm (40 mil) pitch along the line length as shown in Fig. 8d. Two test pad configurations are shown, namely ground-signal-ground (GSG) and GS, and it was found that both gave identical results. The small pads, vias, and thickness, result in reduced interface discontinuities, and thus very fast pulse propagation with wide spectral content. The transmission lines shown in Fig. 7b have 17 x 73.7 μm (0.67 x 2.9 mil) average cross section, with 33.0 μm (1.3 mil) thick ground planes, separated by h_1 = 83.0 μm (3.27 mil) and h_2 = 65.0 μm (2.56 mil) insulator heights. Fig. 9 shows the magnitude of interface discontinuities for various test-pad cases measured with a 35-ps risetime time-domain-reflection (TDR) signal. The waveforms from several different probing positions are shown as follows: for the pads in Fig. 8a, namely at the ends of the extending tabs, or right at the via connection; the use of the pads of Fig. 8b but with 330.2 x 355.6 μm (13x14 mil) pad sizes; the pads of Fig. 8b with 763 μm (30 mil) pads; and finally the same size pads but built on top of a very thick card that has thickness of 3048 μm (120 mil) and relies on 609.6 μm (24 mil) diameter vias. It is evident from these waveforms how crucial the use of the small pads, vias, and thin card structures is for the enhanced extraction. Fig. 8c shows a top view of the parallel-plate structure used to extract the dielectric constant at 1 MHz. Fig. 10 shows an overall view of the measurement setup. The bandwidth of this time-domain measurement technique is expected to be extended with new faster measurement equipment (for example, the 5206-205 differentiator manufactured by Picosecond Pulse Labs and the 70 GHz detector in the 86118A sampling module unit released with the 86100B wide-bandwidth oscilloscope from Agilent Technologies). Extreme care was made in selecting lines that were uniform along their length for all the lengths used and having similar characteristics. The lines were screened using TDR measurements as shown in Fig. 11. Cross sectioning of the measured lines and of the large circular plates was made in three locations to accurately determine the metal and insulator dimensions used in the structure modeling.

The generated models for the card wiring based on the values obtained in Table II and Fig. 4 were used in signal propagation simulations. Both narrow pulse and step-source propagation measurements were compared with the simulations. Dielectric losses become significant mostly on longer lines while short duration pulses propagated on shorter lines highlight the good agreement for the high-frequency fit. Figs. 12 and 13 show the excellent waveform agreement for a pulse propagated on l = 5 cm and a step on l = 20 cm. The agreement in both cases, both in timing and signal amplitude and shape confirm the validity of the generated models and of the entire extraction procedure.

The BT insulator was found to have fairly low dielectric constant of 3.5 – 3.8 that varies only 7.9% from f = 10 KHz to 50 GHz, and tan δ of 0.0013 – 0.0175, that is lower than traditional FR4 materials. The frequency dependence is not very large, as expected for a low loss material dielectric polarization damping. It was also found experimentally, that the BT insulator exhibited only a 0.05% / ^{o}C variation with temperature for ε_r' between T = 25 – 75 ^{o}C. This was obtained by measuring the capacitance of the large circular plate in an enclosed chamber and temperature regulated fixturing. The copper metallization showed a 0.35% / ^{o}C variation of resistivity over the same temperature range. This data was obtained from four-point line resistance measurements.

Effect of Complex Dielectric Extraction

For the BT material, three different cross sections were modeled. The lines had widths of 73.7 um (2.9 mil), 108.9 um (4.29 mil), and 203.2 um (8 mil). The last two widths have 32.0 μm (1.26 mil) thickness. The 108.9 um stripline has 114.0 μm (4.49 mil) dielectric heights while the 203.2 μm stripline has 228.6 μm (9 mil) insulator heights. Attenuations were calculated with and without dielectric loss included and Table III and Fig. 14 show the results. All three different line widths show similar rate of increase of loss due to skin-effect losses governed by a square-root-of-frequency dependence. The thicker and wider 203.2 μm lines show the transition to dielectric-loss dominated region starting from a much lower frequency of about 2 GHz, compared to the other more resistive lines. The rate of increase in attenuation is much more rapid

in this case and highlights the importance of having accurate extraction of the dielectric loss values for the higher frequency operation requirements. 3-6 GHz clock frequencies will be transmitted on long card wiring in the near future. Such demands imply the use of larger card cross sections together with lower loss materials as analyzed in this paper.

Simulations were performed to assess the maximum usable length for 6 GHz clock frequencies or 166-ps-wide pulses. The risetime used was one third of the bit time or 50 ps. 1.5 pF discontinuities were added at both ends of the line. The receiving end of the line had a 50 Ω termination, and the source had 30 Ω impedance. The 650 mV peak amplitude of the pulse was the criterion used for all cases for an input of 0.977 V at the beginning of the line or 3.53 dB attenuation. These numbers roughly correspond to a 90-nm CMOS process. Simulations are shown in Fig. 15 for the case with and without dielectric loss. The results highlight the large effect dielectric loss has at higher frequencies and for wider lines with lower resistive losses. While for the 2.9-mil case, dielectric loss only reduces the usable length by 21%, for 4.29-mil case the loss is 40%, and for 8-mil case the loss is 55%. Table IV also shows similar results with a larger driver size having 10 Ω impedance. It should be noted that the use of equalization or pre-emphasis can significantly increase these lengths but the effect of dielectric loss on the total line loss will remain the same.

Conclusions

A simple measurement technique was shown that allows the broadband extraction of both the dielectric constant and dielectric loss for representative card wiring. Unlike the general practice in the industry, it is a time-domain technique that uses typical transmission line structures built with specially designed test pads and via configurations. Using this technique, new materials, with lower dielectric loss were analyzed over the 10 KHz to 50 GHz range. This wide frequency range for the extraction of the complex permittivity was made possible by the use of a simple, physically consistent, fitting algorithm and extrapolation. The time-domain technique uses short-pulse measurements, signal processing of digitized data, and iteration of modeling and measurement with comparison of attenuation and phase constant. This procedure is augmented with additional, low-frequency, parallel-plate capacitance measurements to generate consistent broadband models. Line resistance and low-frequency line capacitance measurements, as well as accurate sample dimensions are also needed. The technique allows generation of fully-causal transmission-line models up to 50 GHz. Such wide bandwidth is essential for the accurate design of multi-GHz data-rates transmitted on printed-circuit board wiring. The technique is limited by the practical manufacturing capabilities, the resistive and dielectric losses of the structures of interest, the bandwidth of the test set-up, and the inherent signal-to-noise ratio of the time-domain technique. Nevertheless, the real strength of the technique is the ability to obtain broadband models for structures that are representative of actual practical configurations used in high-performance computer systems using only limited measurement data. Signal propagation measurement and simulations highlighted the need for such broadband extraction.

Acknowledgement

The authors would like to thank Dylan Williams from National Institute of Standards and Technology for the valuable recommendations made in the design of the transmission lines used in the test vehicle that helped make possible the extended bandwidth measurements shown in this paper.

References

[1]. A. E. Ruehli, A. C. Cangellaris, "Methodologies for the electrical modeling of interconnects and electronic packages", Proceedings of IEEE, vol. 89, no.5, pp.740-771, May, 2001.

[2]. K. M. Coperich, J. Morsey, A. C. Cangellaris, A. Ruehli, " Physically consistent transmission line models for high-speed interconnects in lossy dielectrics", *Proc. IEEE 10th Topical Meeting on Electrical Performance of Electronic Packaging, EPEP'01,* pp. 247-250, Oct. 29-31, Cambridge, MA, 2001.

[3]. J. Baker-Jarvis, R. G. Geyer, J. H. Grosvenor, Jr., M. D. Janezic, C. A. Jones, B. Riddle, C. M. Weil, "Dielectric Characterization of Low-loss Materials, A Comparison of Techniques", *IEEE Trans. on Dielectrics and Electrical Insulation*, vol. 5, no. 4, pp.571-577, Aug. 1998.

[4]. A. R. Djordjevic, R. M. Biljic, V. D. Likar-Smiljanic, T. K. Sarkar, "Wideband frequency0domain characterization of FR-4 and time-domain causality", *IEEE Trans. Electromag. Compatibility*, vol. 43, no.4, pp.662-667, Nov. 2001.

[5]. C. Svenson, G. E. Dermer, "Time domain modeling of lossy interconnects", *IEEE Trans. Advanced Packg.*, vol. 24, no. 2, pp.191-196, May 2001.

[6]. M. D. Janezic, D. F. Williams, V. Blaschke, A. Karamcheti, C. S. Chang, "Permittivity Characterization of Low-k Thin Films From Transmission-Line Measurements", *IEEE Trans. Microwave Theory Tech.*, vol. 51, no. 1, pp.132-136, January 2003.

[7]. A. Deutsch, G. Arjavalingam, G. V. Kopcsay, "Characterization of resistive transmission lines by short-pulse propagation", *IEEE Microwave Guided Wave Lett.*, vol. 2, pp.25-27, Jan. 1992.

[8]. Nelco N4000 laminates are manufactured by Park/Nelco, a subsidiary of Park Electrochemical Corporation, http://www.parknelco.com/.

[9]. A. Deutsch, M. R. Scheuermann, G. Arjavalingam, L. Kneller, J. K. Tam, and C. W. Surovic, " Characterization of resistive transmission lines to 70 GHz with ultrafast optoelectronics", *IEEE Microwave and Guided wave Lett*., vol. 3, pp. 75-77, 1993.

[10]. A. Deutsch, G. V. Kopcsay, P. W. Coteus, C. W. Surovic, P. E. Dahlen, D. L. Heckmann, D.-W. Duan, "Frequency-dependent losses on high-performance interconnections", *IEEE Trans. Electromag. Compatibility*, vol. 43, no. 4, pp. 446-465, Nov. 2001.

TABLE I
Initial Dielectric Loss Values

Freq. (GHz)	tan δ
0.00001	0.0050
0.00010	0.0060
0.00100	0.0070
1.00000	0.0070
2.15444	0.0070
3.17000	0.0100
4.64160	0.0150
10.0000	0.0150
21.5444	0.0150
46.4160	0.0150

TABLE II
Extracted Dielectric Constant and Loss Values

Freq. (GHz)	ε_r	tan δ
0.00001	3.8136	0.00128
0.00010	3.7914	0.00520
0.00100	3.7500	0.00700
0.01000	3.7119	0.00700
0.10000	3.6742	0.00700
1.00000	3.6354	0.00700
2.15444	3.6346	0.00702
3.17000	3.6325	0.01073
4.64160	3.6186	0.01500
10.0000	3.5777	0.01750
21.5444	3.5458	0.01750
26.0000	3.5383	0.01750
46.4160	3.5148	0.01750
50.0000	3.5119	0.01750
Infinite	3.3412	

TABLE III
Calculated Attenuation With and Without Dielectric Loss

Freq.	Width=73.7 μm		Width=109.2 μm		Width=203.2 μm	
	tanδ	tanδ=0	tanδ	tanδ=0	tanδ	tanδ=0
(GHz)	(dB/cm)		(dB/cm)		(dB/cm)	
1.50	0.1168	0.1021	0.0769	0.0617	0.0498	0.0345
3.00	0.1953	0.1443	0.1388	0.0872	0.1007	0.0488
6.00	0.3762	0.2046	0.2959	0.1233	0.2420	0.0692
10.0	0.5619	0.2645	0.4585	0.1595	0.3894	0.0895

TABLE IV
Maximum Usable Length for 6 GHz

	Zdrv=10Ω		Zdrv=30Ω	
	tanδ	tanδ=0	tanδ	tanδ=0
Width (μm)	Length (cm)			
73.7	24.4	32.4	22.0	28.0
109.2	31.5	52.1	29.0	48.0
203.2	42.3	91.3	37.0	82.0

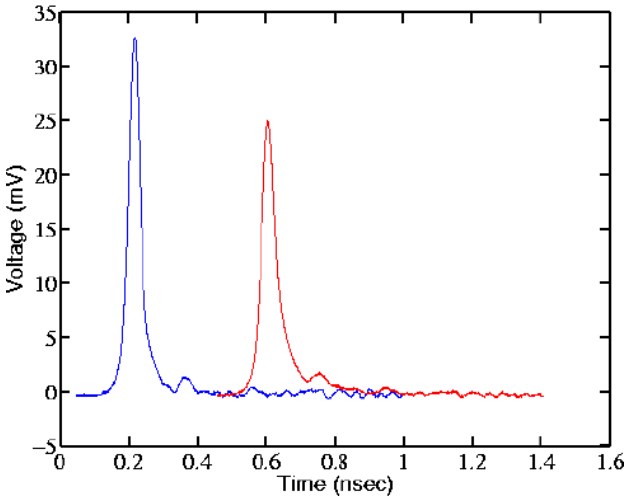

Fig. 1 Measured propagated pulse response for l = 2 cm and l = 8 cm printed circuit board wiring with BT insulation.

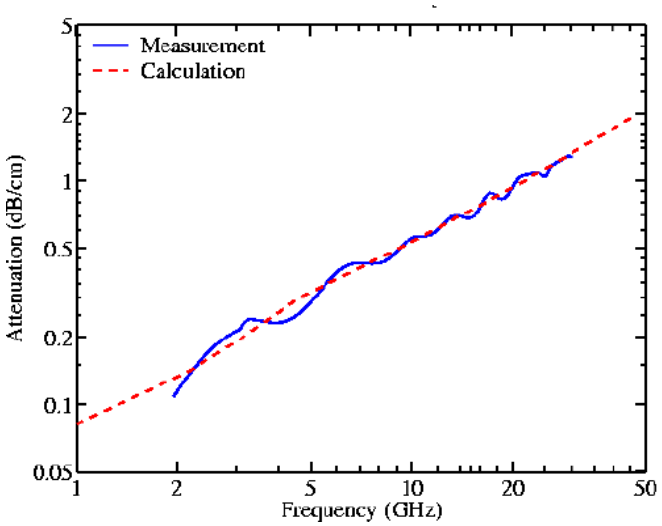

Fig. 2 Measured and calculated attenuation using the short-pulse propagation technique with 1-cm, 2-cm, 5-cm, 8-cm, 9.8-cm long wiring.

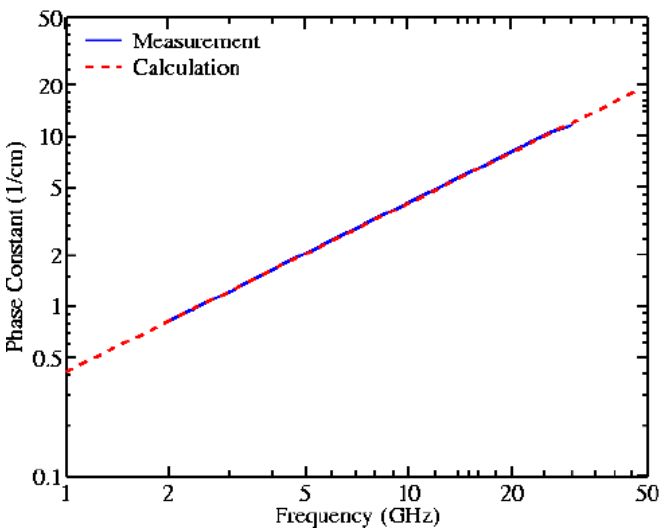

Fig. 3 Measured and calculated phase-constant using the short-pulse propagation technique with 1-cm, 2-cm, 5-cm, 8-cm, 9.8-cm long wiring.

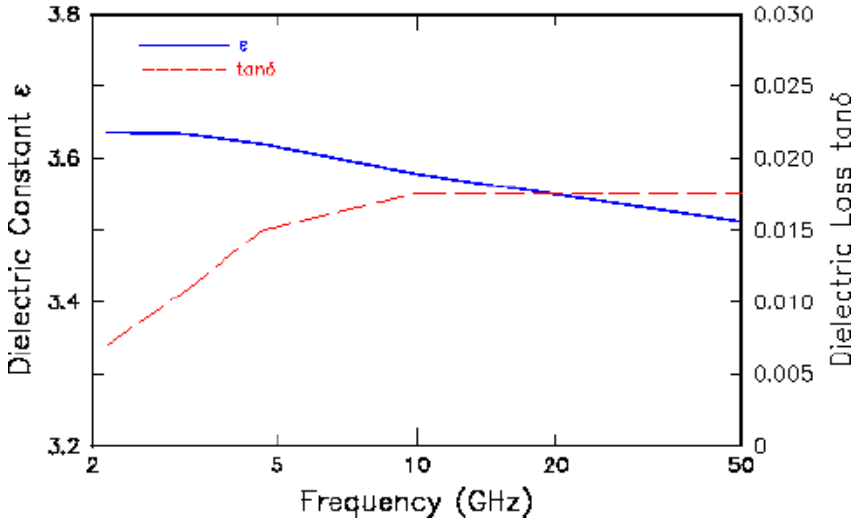

Fig. 4 Extracted dielectric constant and dielectric loss variation with frequency.

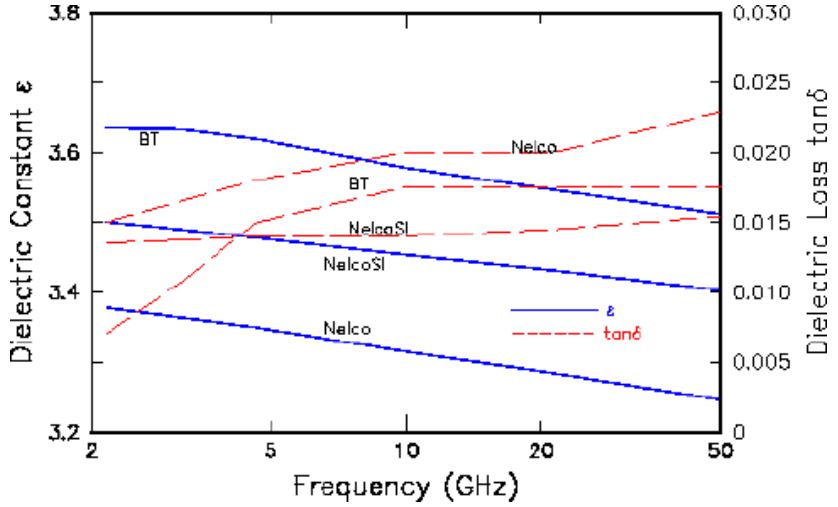

Fig. 5. Extracted dielectric constant and dielectric loss variation with frequency for BT, Nelco N4000-13, and Nelco N4000-13SI materials.

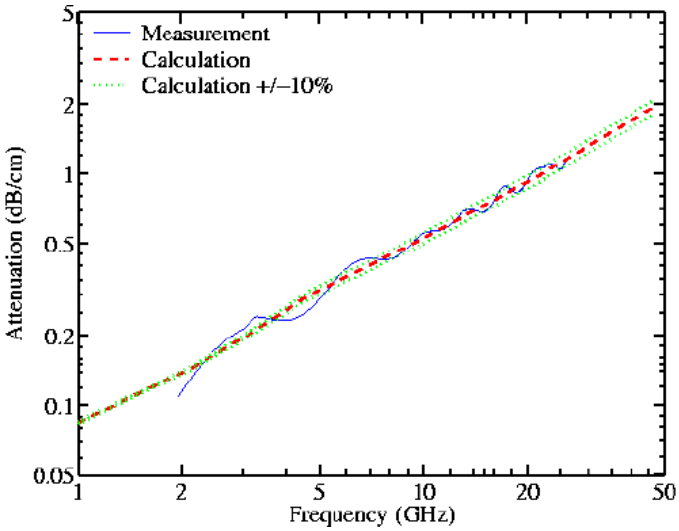

Fig. 6. Measured and calculated attenuation. The dotted traces use tanδ values that are +/-10% above and below the initial values in Table I

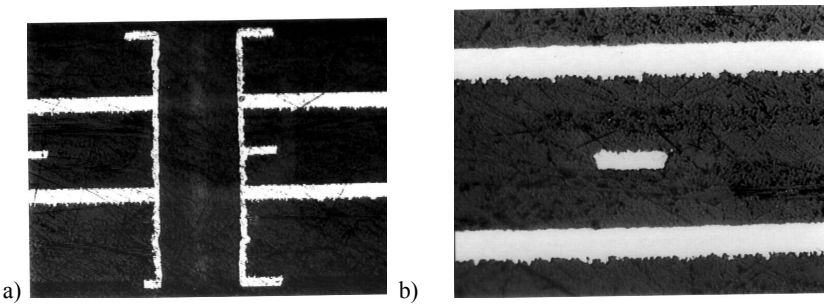

Fig. 7 a) Cross section of 8-mil-diameter via connecting the top and bottom metal layers to the stripline wiring between two ground planes; b) cross section of signal layer wiring and top and bottom ground planes.

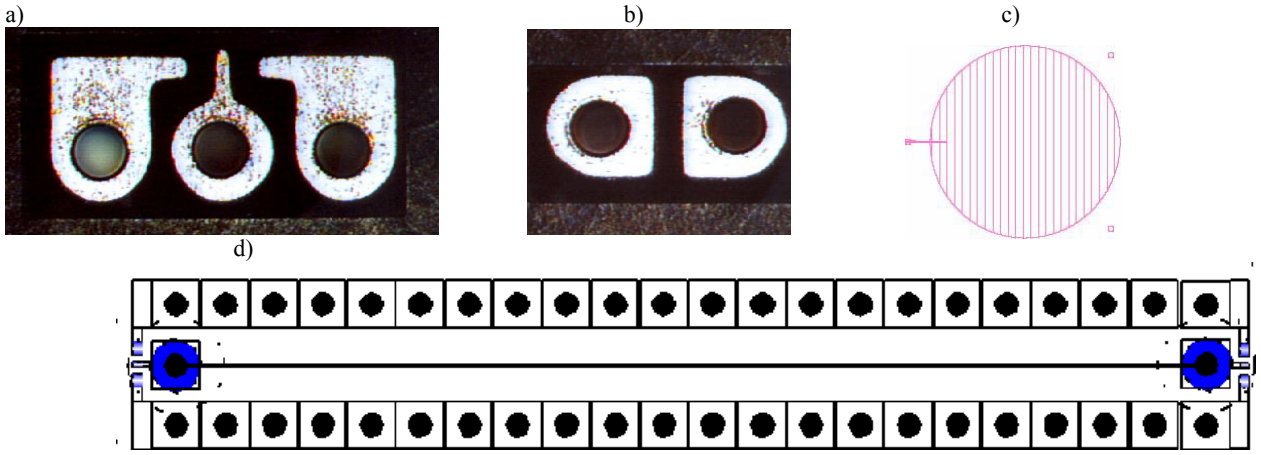

Fig. 8 Layout of a) GSG end pads on 16 mil pitch with 8 mil vias, b) GS end pads, 13 x 14 mil, on 17 mil pitch and c) layout of the 500-mil-diameter circular plate placed on the signal layer between the top and bottom ground planes, and d) signal layer transmission lines showing the vias along the length on 40 mil pitch and the very small GSG test pad configuration on the top surface.

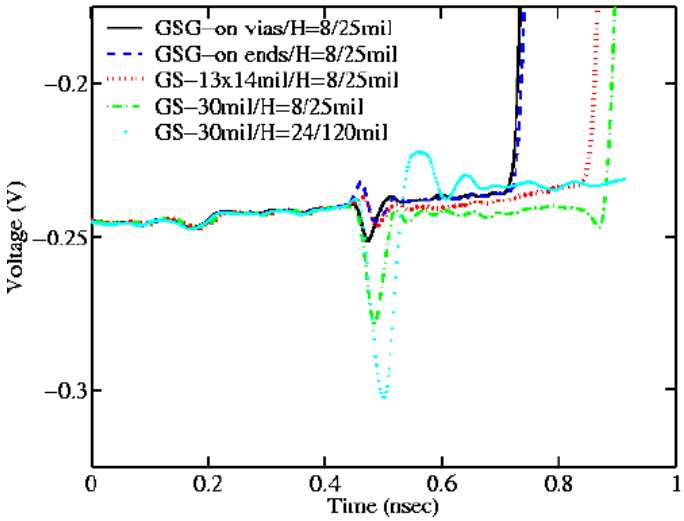

Fig. 9 TDR response for five different test pad configurations. Solid trace for pad configuration in Fig. 8a with probes touching at the 8-mil-diameter via locations, dashed trace for Fig. 8a pads with probes touching at small pad extensions of Fig. 8a, dotted trace for same pads as in Fig. 8b of 13 x 14 mil in size and using 8-mil vias, dot-dashed trace for same type of pads as in Fig. 8b with 30 x 30 mil size and 8-mil vias, dotted trace with largest discontinuity for pads of the type of Fig. 8b, with 30 x 30 mil size, on 120-mil thick card using 24-mil diameter vias.

Fig. 10 Test measurement set-up showing the differentiator in-line with the sampling oscilloscope step source and the coaxial probes using for probing the various lengths lines.

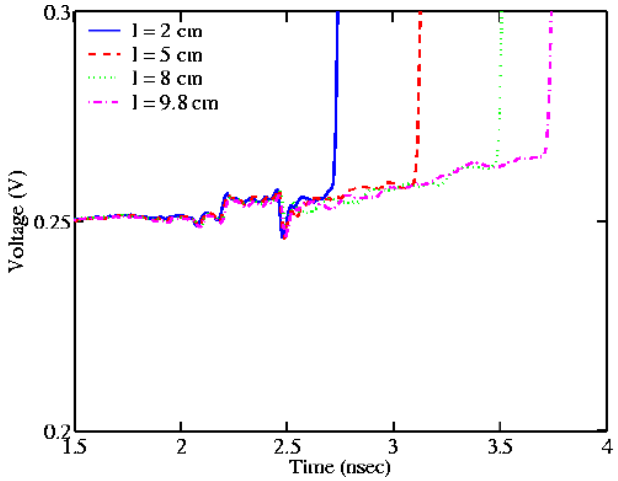

Fig. 11 TDR response for lines of 2, 5, 8, and 9,8 cm lengths using a 35-ps step source with 250-mV amplitude .

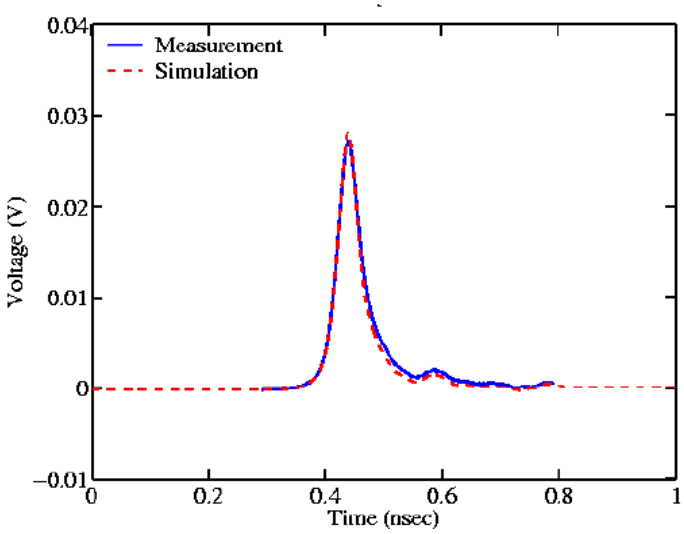

Fig. 12. Measured and simulated propagated pulse on 5 cm long transmission lines using the extracted parameters of Fig. 4.

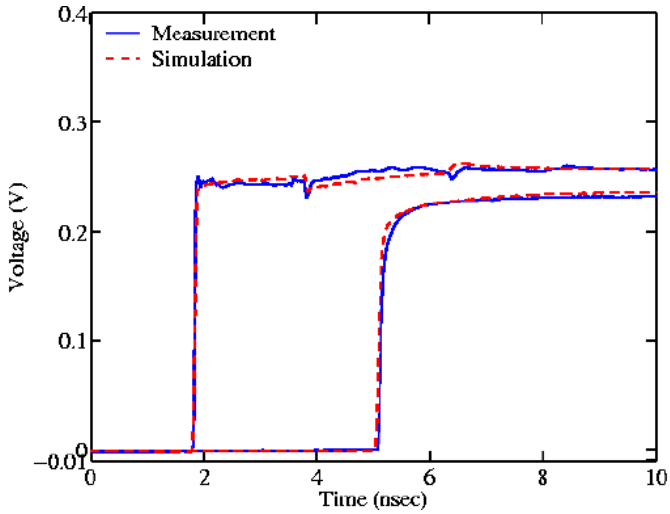

Fig. 13. Measured and simulated propagated pulse on 20-cm- long transmission lines using the extracted parameters of Fig. 4. Step-source excitation was used with 35 ps rise-time, and 250 mV amplitude. Measured and simulated delays were 1.286 ns and 1.280ns, respectively.

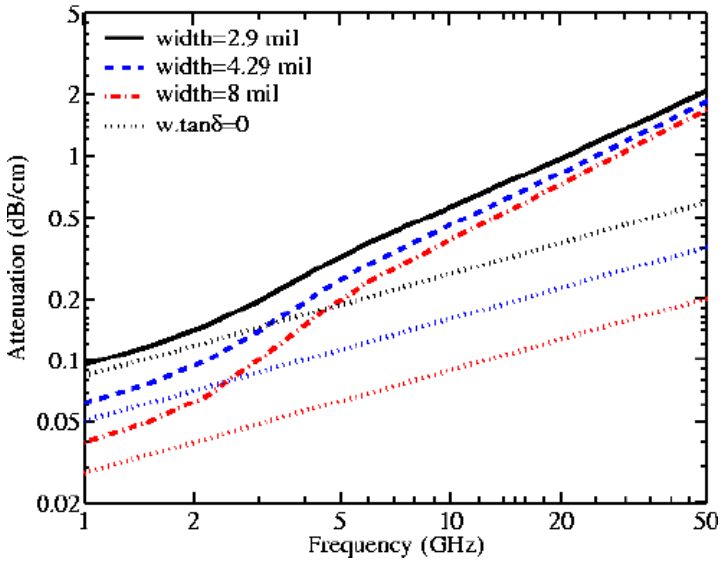

Fig. 14. Calculated attenuation with BT insulator for 2.9, 4.29, and 8-mil wide lines, with and without dielectric loss. All the dotted traces are for calculations without dielectric loss.

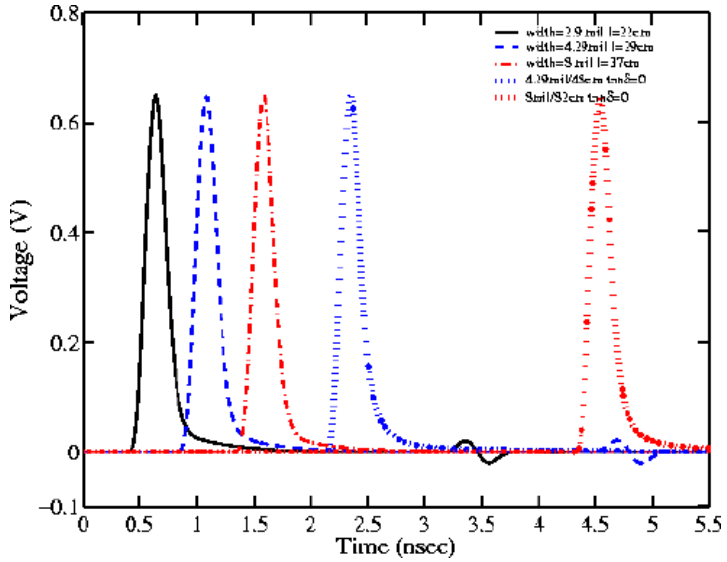

Fig. 15. Propagated pulses for 6 GHz frequency (166-ps-wide pulses) for lines having 2.9, 4.29, and 8.0 mil widths. The dotted traces show the pulses for 4.29 and 8-mil wide lines simulated without dielectric loss for l = 48 cm and 82 cm, respectively. The input source has 0.977 V amplitude in all cases and the results are also listed in Table IV for the same propagated amplitude of 650 mV. The source has 30 Ω impedance, 50-ps rise-time, and the lines are terminated with 50 Ω. Total capacitive load for beginning and end of the wiring is 3 pF. Solid trace is for width = 2.9 mil, l = 22 cm, dashed trace is for width = 4.29 mil, l = 29 cm, dot-dashed trace is for width = 8 mil, l = 37 cm.